NeuroImage 328 (2026) 121784

Contents lists available at ScienceDirect

NeuroImage

journal homepage: www.elsevier.com/locate/ynimg

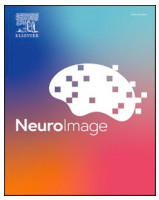

The neurophenomenology of a self-induced transcendental visionary state: A case study

Gabriel Della Bella [a,b,1,*], Agustina Velez Picatto [a,1], Dante Sebastián Galván Rial [a], Sebastián Cukier [c], Gustavo Foa Torres [d], Magaly Catanzariti [e], Diego Mateos [e,f,g], Pedro Lamberti [b], Etzel Cardeña [h,2], Pablo Barttfeld [a,2]

[a] Cognitive Science Group, Instituto de Investigaciones Psicológicas (IIPsi, CONICET-UNC), Facultad de Psicología, Universidad Nacional de Córdoba, Córdoba, Argentina.
[b] Facultad de Matemática, Astronomía, Física y Computación, Universidad Nacional de Córdoba, Córdoba, Argentina.
[c] Hospital Elizalde, Casa Cuna, Buenos Aires, Argentina.
[d] Instituto Oulton, Córdoba, Argentina.
[e] Instituto de Matemática aplicada del Litoral (IMAL-CONICET-UNL), Santa Fe, Argentina.
[f] Universidad Autónoma de Entre Ríos (UADER), Entre Ríos, Argentina.
[g] Achucarro Basque Center for Neuroscience, Leioa Bizkaia, Spain.
[h] Center for Research on Consciousness and Anomalous Psychology (CERCAP), Department of Psychology, Lund University, Lund, Sweden.

ARTICLE INFO

Keywords:
Non-ordinary states of consciousness
fMRI
Connectivity
Single case

ABSTRACT

Non-ordinary states of consciousness (NOC) offer a way to examine how large-scale brain dynamics reorganize as experience changes. We studied a participant able to reliably enter a self-induced NOC state characterized by vivid imagery, altered bodily perception, and a sense of unity. Across 20 fMRI sessions, we measured functional connectivity in four conditions (Baseline, Transition, NOC, and Residual) and compared the results with a matched control group. During the Transition phase, connectivity became more variable, indicating a temporary destabilization of network organization. In the NOC state, inter-network connectivity decreased broadly, with visual cortex showing reduced coupling to auditory, sensorimotor, orbitofrontal, thalamic, and cerebellar regions, and the somatomotor-dorsal network disengaging from auditory and language cortices, paralleling the reported visual phenomena and changes in bodily experience. In contrast, frontoparietal and salience networks showed increased coupling with precuneus/posterior cingulate, multimodal temporal cortex, and cerebellar hubs, in agreement with subjective reports of sustained inward-directed attention and stable absorption. Entropy and complexity analyses revealed systematic shifts that tracked the experiential sequence and returned to baseline in the Residual condition. This single-case study brings together something uncommon: controlled experimentation, voluntary induction of NOC states, and rich phenomenological data. Taken together, these elements offer a strong foundation for neurophenomenological research and illustrate why pairing structured paradigms with lived experience is useful for understanding non-ordinary states of consciousness.

1. Introduction

Non ordinary states of consciousness (NOC), defined as mental states that differ qualitatively from ordinary waking experience (Tart, 1976; Timmermann et al., 2023), arise across a wide range of human experiences and are receiving increasing attention in neuroscience (Fort et al., 2025; Gosseries et al., 2024). Pharmacologically induced NOC, especially those obtained with anaesthetics and psychedelics, have been central to identifying large scale neural signatures of NOC. These models, however, present several limitations. Anaesthesia-based approaches often emphasise global markers of conscious level rather than the structure of conscious contents. Psychedelic states pose different challenges: the timing and trajectory of the experience cannot be easily controlled or aligned across sessions or participants, the most intense

* Corresponding author.
E-mail address: dellabellagabriel@gmail.com (G. Della Bella).
[1] First author.
[2] Last author.

https://doi.org/10.1016/j.neuroimage.2026.121784
Received 20 December 2024; Received in revised form 28 November 2025; Accepted 4 February 2026
Available online 4 February 2026

phases tend to show reduced reportability, and their overall reproducibility of phenomenology is very limited (Timmermann et al., 2023). Also, pharmacological induction involves physiological changes caused by the drug itself, which complicates the interpretation of neural effects (Barttfeld et al., 2015; Stamatakis et al., 2010). Together, these limitations constrain the granularity with which phenomenology can be related to neural dynamics and hinder efforts to link the richness of conscious experience to its moment-to-moment neural organisation (Timmermann et al., 2022, 2023).

Voluntarily induced NOCs offer a complementary approach. Practices such as deep absorption, meditative concentration, hypnosis and certain forms of trance show that some individuals can intentionally enter NOCs while preserving awareness and moving through a recognizable temporal progression (Berkovich-Ohana, 2015; Cardeña, 2005; Cardeña et al., 2013; Deeley et al., 2013). These states make possible the study of NOC without pharmacological perturbations and without loss of behavioural control. However, their phenomenology often varies across episodes and across practitioners, and reproducibility at the level of internal phases or trajectories has rarely been demonstrated, and the risk is to study a collection of isolated, highly idiosyncratic states and to obtain neural correlates without a coherent structure or predictive power. As a result, we still know little about the neural dynamics that support their respective NOCs, and even less about their temporal organisation.

This tension between models that offer strict experimental control at the cost of phenomenological richness, and models that offer rich experiences at the cost of control and reproducibility, has made it challenging to develop frameworks capable of mapping complex experiences onto precise neural dynamics, the neurophenomenological goal. The present study aims to address this gap by combining a systematic and reproducible framework, organised into four defined and repeatable phases inspired by anaesthesia research (Barttfeld et al., 2015; Chennu et al., 2016), with the experiential richness of a voluntary self-induced NOC.

We examined a self-taught participant capable of intentionally entering a NOC state that can be reliably reproduced across scanning sessions, with a phenomenology that overlaps with features described in psychedelic, hypnotic and trance, such as visual imagery, altered embodiment, shifts in time perception and ego attenuation. The state includes features such as vivid internal imagery, alterations of body schema, changes in agency and a sense of unity, while retaining a high degree of voluntary control and temporal stability (Cardeña et al. 2025). Across four fMRI conditions (Baseline, Transition, NOC, and Residual), we analysed functional connectivity and signal complexity, complemented by a micro-phenomenological interview and detailed post-session reports. Based on the literature, we hypothesised that the NOC state would involve reduced inter-network connectivity, increased connectivity within frontoparietal and default mode systems, a rise in connectivity variability during the transition phase and systematic changes in entropy and complexity across conditions. Taken together, these elements provide an opportunity to examine how a self-induced NOC reorganises large-scale brain dynamics across well-defined experiential phases.

2. Materials and methods

2.1. Participants

The main participant is a 37-year-old woman (author AVP) with the ability to self-induce a NOC known as a visionary transcendental state. This label, introduced by (Cardeña et al., 2025), refers to a sequence of experiential modes within NOCs that progress from vivid visionary imagery to transcendental or unitive awareness. Such states typically involve luminous and often symbolically charged visual forms, heightened absorption with reduced sensory input, dissolution of perceptual and ego boundaries, a sense of timelessness, and an encompassing feeling of connection or merging with a larger reality. In AVP, this trajectory unfolds spontaneously and reproducibly across sessions: it begins with intricate geometric and luminous imagery and culminates in a lucid, expansive state of unity and serenity, closely matching the phenomenological continuum described in the taxonomy. At the time of data collection, she was not involved in the study design, hypothesis formulation, data analysis, or interpretation. She was blinded to the specific aims of the study and participated solely as a volunteer. All data preprocessing, connectivity analyses, and statistical procedures were conducted independently by the research team and completed before any results were shared with her. Her inclusion as an author reflects her substantial contribution to the neurophenomenological interpretation of the findings, particularly through detailed introspective reports and participation in a micro-phenomenological interview.

The absence of clinical criteria for psychiatric disorders (based on DSM-5-TR) was confirmed through an open psychiatric interview (conducted by author SC). A semi-structured interview was used to complete the Positive and Negative Syndrome Scale (PANSS) (Kay et al., 1987), specifically aiming to rule out schizophrenia or other psychotic disorders due to the presence of sensory-perceptual alterations. We ruled out anxiety disorders, mood disorders, psychotic disorders, obsessive-compulsive spectrum disorders, trauma-related disorders, dissociative disorders, sleep-wake disorders, conduct disorders, substance-related disorders, personality disorders, neurodevelopmental disorders, and medication-induced disorders. The participant was in good health and reported no medical conditions other than compensated hypothyroidism treated with levothyroxine.

The participant did not receive formal training in techniques for inducing non-ordinary states of consciousness. Her practice developed intuitively and independently from early adolescence, as part of a sustained curiosity about the nature of perception and consciousness. At age 24 she experienced a spontaneous visual phenomenon (a yellow shape projected onto a blank surface) that she later learned to reproduce voluntarily through self-guided experimentation. Over time, she progressively refined this ability through reasoning and introspection, rather than through any specific contemplative or meditative method. This practice has since become a continuous mode of perception and inquiry rather than a discrete daily exercise. She also reports stable associations between letters, numbers, and colors (e.g., perceiving “S” as yellow and “T” as green), consistent with mild grapheme-color synesthesia present since childhood.

A control group of ten female volunteers, matched to AVP in age and level of education (Table S1) was included. Controls met the same inclusion criteria (absence of neurological or psychiatric conditions and overall good health), assessed through self-report and brief interviews. All controls underwent the same MRI protocol as AVP. Participants were recruited using snowball sampling through social media. All participants read and signed the information and consent form provided by the ethics committee that approved the project (Ethics Committee of the Institute of Psychological Research, CONICET Córdoba). All data collections and analyses were carried out in accordance with the Declaration of Helsinki.

2.2. Psychological assessment

AVP was interviewed multiple times by one of the authors with expertise in phenomenological methods (EC). A micro-phenomenological interview (Petitmengin, 2006) was conducted focusing on one of her experiences during scanning, using open-ended questions (see Supplementary Information). In addition, AVP produced detailed written notes after each session. These reports, summarized in Table S2, indicated consistent induction of the core NOC with moderate session-specific variation.

2.3. Brain imaging

AVP completed 20 MRI sessions, each organized into four distinct blocks (Fig. 1a). Sessions were collected over a period of five months (March to July, 2023, with a typical interval of one week between sessions. This number of sessions was chosen to obtain a statistically meaningful sampling of both the stable and variable components of the self-induced state, while remaining feasible for the participant, who committed to a demanding schedule without compromising her well-being. All sessions were conducted under highly comparable conditions (same time of day, same scanner environment, eyes closed at rest). The participant reported stable induction ability across sessions, no signs of fatigue or habituation, and no episodes of drowsiness or sleep.

A Siemens Spectra 3 Tesla MRI machine, with 16 channel head coil, was used to obtain 36 ascending interleaved slices (TR = 3000 ms, TE = 30 ms, flip angle 90°). We also collected T1-weighted structural images with 1×0.488×0.488 mm resolution, using an MPRAGE sequence with TR = 1620 ms, TI = 900 ms, TE = 2.42 ms and flip angle = 9°. Each session consisted of four functional blocks, each lasting 7:30 minutes, and a structural block, organized as follows: the first block was a *Baseline* condition (common resting state), the second block was labeled *Transition* (where AVP began to alter her mental state), the third block was *NOC*, and the fourth block was *Residual* (AVP attempted to return to Baseline but remained in a partially altered state that no longer matched the NOC yet had not fully resolved into ordinary wakefulness). During Transition, AVP signaled having crossed the subjective threshold into the NOC using a small foot movement. In the Residual, she was asked to move her foot at a random moment to provide a control movement condition. To ensure this did not affect analyses, connectivity was recomputed after removing the three volumes before and after the movement; results were unchanged (r = 0.99; Fig. S1).

Between blocks, an experimenter entered the MRI room to cue the next condition except between the Transition and NOC to avoid distractions. The T1 image was collected between the third and fourth blocks to allow recovery time.

Control participants followed the same protocol but were instructed to maintain eyes closed and generate visual imagery during the second and third blocks (corresponding to Transition and NOC in AVP). One control participant did not complete the Baseline; another had corrupted data in the third block. Authors GDB, DSGR and PB collected all data.

2.4. Image preprocessing

Images were preprocessed using CONN (Whitfield-Gabrieli and Nieto-Castanon, 2012) version 21.a standard preprocessing pipeline. The steps applied were: realignment and unwarping for motion correction, slice timing correction, corregistration to the T1 image, segmentation, normalization to the standard MNI space, and smoothing at 8 mm FWHM. Denoising included white-matter and CSF components and motion regressors using aCompCor, followed by band-pass filtering (0.008 - 0.09 Hz) and linear detrending.

Functional images were parcelated into 300 spherical Regions of Interest (ROIs) from the Greene Lab atlas (Seitzman et al., 2020), grouped into 14 functional networks (Fig. 1b). This atlas was selected because it provides fine-grained and anatomically well-defined coverage of the entire brain, including cortical, subcortical, and cerebellar regions, enabling whole-brain analyses of large-scale reconfigurations. Its explicit assignment of each ROI to well-characterized networks makes it particularly suitable for quantifying intra- and inter-network connectivity and for detecting network-specific modulations. This atlas labels one of the networks and its 12 associated ROIs as "unassigned". They were excluded from all analyses leaving a total of 288 ROIs and 13 networks. The networks included in the atlas are: dorsal attention (DA), medial temporal lobe (MTL), default mode network (DMN), reward (Rew), salience network (SN), fronto-parietal (FP), somatomotor dorsal (SMD), somatomotor lateral (SML), ventral attention (VA), cingulo-opercular (CO), visual (VIS), auditive (AUD) and parieto-medial (PM). All analyses were conducted on the functional time series data from these 288 ROIs.

2.5. Connectivity per functional network

We estimated the connectivity between and within functional networks. Except stated otherwise, all 20 sessions were analyzed independently to estimate connectivity, entropy, and complexity measures before averaging across sessions for each condition. For each session and condition, we estimated brain connectivity by calculating the Pearson correlation between pairs of time signals. This resulted in a 288×288 matrix per participant and experimental condition (Fig. 1c, d). We defined two types of connectivity: intra-network (within the same network, averaging the correlation values of the submatrix corresponding to a single network, Fig. 2a, left) and inter-network (between regions of different networks, averaging all correlation values of the

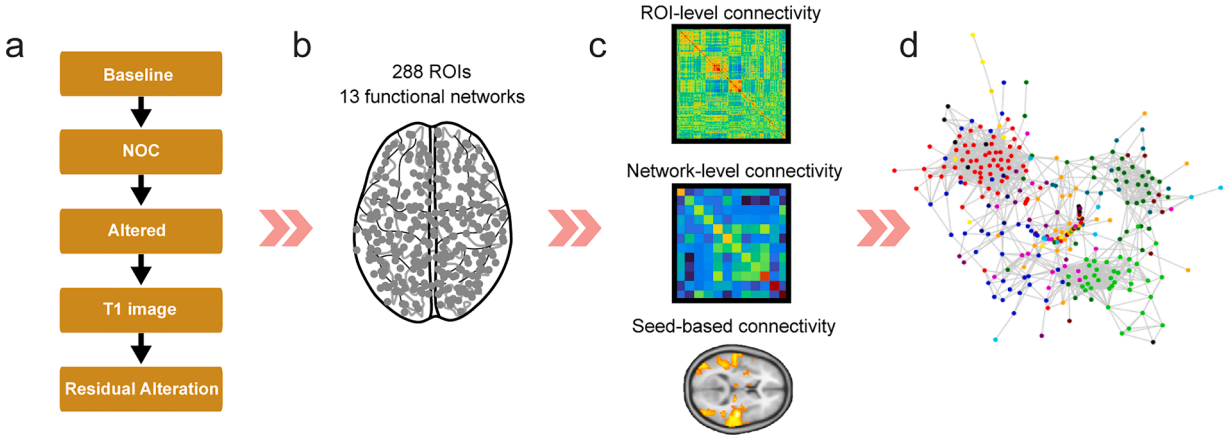

Fig. 1. Analysis pipeline. a) Experimental design: The participants underwent MRI sessions consisting of four functional blocks and one structural block (placed between the NOC condition and the Residual condition to allow the participants to return to the Baseline). b) We parceled the brain into 288 regions of interest, from which we constructed correlation matrices based on ROIs or functional networks. All studied metrics were calculated from these matrices. c) We computed the functional connectivity at the network level and the ROI level, as well using a seed analysis. Within the ROI level, we distinguished between intra-network connectivity (connectivity among ROIs of the same network) and inter-network connectivity (connectivity among ROIs of different networks). d) We used intra-network and inter-network functional connectivity to study topographical changes in our participant and the control group using linear mixed models and force-directed graph projections.

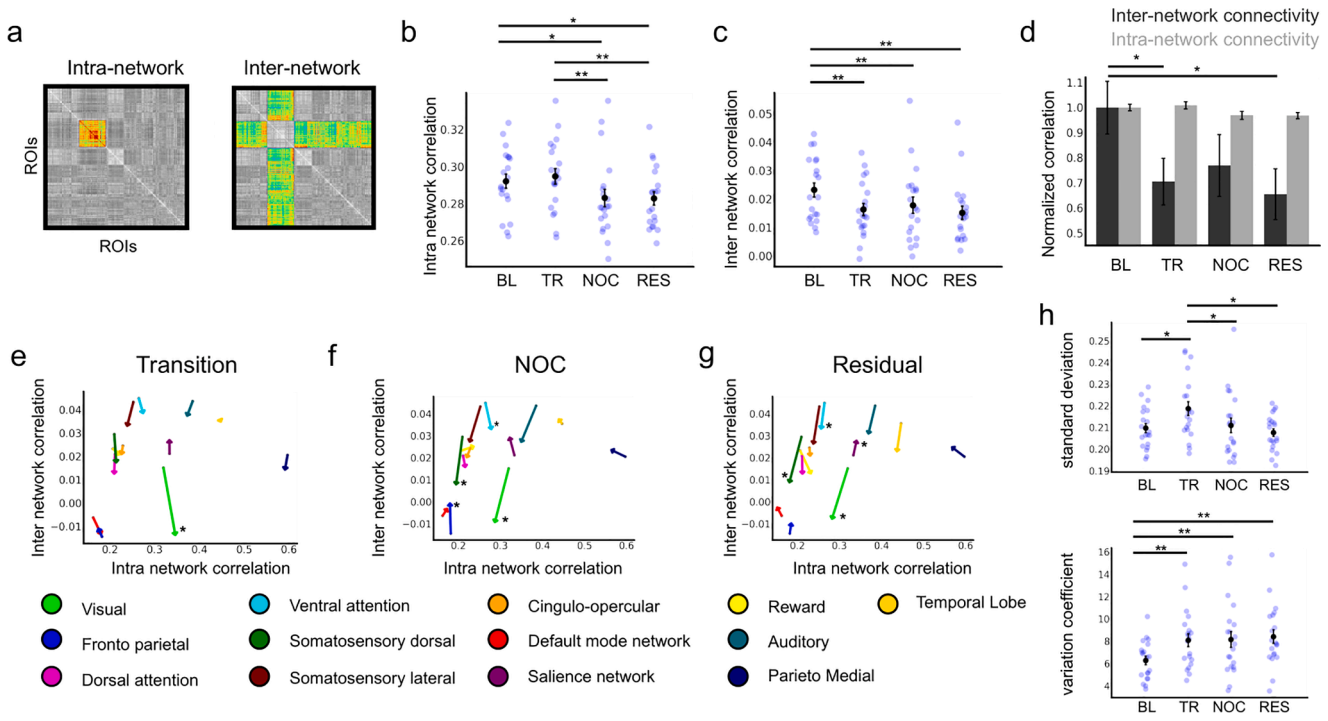

Fig. 2. Global connectivity changes. a) Example matrices of how we calculated intra-network functional connectivity (left) and inter-network connectivity (right). Intra-network functional connectivity is defined as the average correlation values between ROIs of the same functional network. Inter-network connectivity is defined as the average correlation values between ROIs *i* and *j* such that *i* belongs to one functional network and *j* belongs to another functional network. b) Intra-network connectivity for each experimental condition. Individual points represent AVP's sessions, and the bars denote the standard error of the mean (S.E.M.). An asterisk indicates $p < 0.05$, and two asterisks indicate $p < 0.01$, both FDR corrected. NOC and Residual conditions are significantly different from Baseline. c) Inter-network connectivity for each experimental condition. Individual points represent AVP's sessions, and the bars denote the S.E.M. All conditions differ significantly from Baseline. d) Intra- and inter-network connectivity normalized to Baseline. Intra-network connectivity remains almost unchanged across conditions, while inter-network connectivity decreases significantly, suggesting a dissolution of inter-network relationships and maintenance of functional networks. e-g) Two-dimensional maps showing changes in intra-network connectivity (x-axis) and inter-network connectivity (y-axis). The base of the arrow represents the intra- and inter-network pair characterizing the Baseline, while the arrow's endpoint marks the value in each experimental condition. Thus, the arrow's magnitude indicates the change between the specified condition and Baseline. Asterisks indicate $p < 0.05$. The nodes corresponding to functional networks whose connectivity changes across conditions were statistically significant were colored using the FN's specific color. h) Standard deviation (top) and Coefficient of Variation (bottom), as a proxy for absolute and relative functional connectivity variability.

submatrices corresponding to pairs of ROIs from one network and all others, Fig. 2a, right) and calculated each of them across the four conditions (Fig. 2b, c).

We calculated a normalized correlation, defined as the inter- or intra-network correlation divided by the corresponding Baseline average (Fig. 2d). Specifically, the inter-network correlation is divided by the average inter-network correlation at Baseline, and, similarly, the intra-network correlation is divided by the average intra-network correlation at Baseline.

To gain a clearer understanding of the intra- and inter-network correlation dynamics, we plotted each network's connectivity on a 2D plane (Figs. 2 e-g and S3), with inter-network correlation on the y-axis and intra-network correlation on the x-axis. Each point represents an (intra, inter) pair correlation at the Baseline. We drew arrows from the Baseline to the corresponding inter- and intra-network values for each condition. Longer arrows indicate larger changes in correlation compared to the Baseline condition, and the direction of the arrow illustrates whether the change was primarily in the inter- or intra-network correlations.

We also used both the standard deviation (Fig. 2h, top) and the coefficient of variation (CV) (Fig. 2h, bottom), calculated as the standard deviation of the average correlation values per ROIs divided by their mean, for each subject or session and condition. CV quantifies the relative variability of connectivity, providing a measure of the dispersion of correlation values in relation to their mean. A high standard deviation or CV suggests that the connections between brain regions are unstable and exhibit high variability, indicating that functional connectivity in that condition or participant is inconsistent. Conversely, a low CV suggests that the connections are more stable and consistent, with less relative variability.

To compare connectivity changes across conditions, we calculated the differences between the full 288-ROI correlation matrices for each condition. We then averaged these differences within each network to obtain a single value per functional network. This value represents the average difference in connectivity for that network between a given condition and Baseline. We quantified these differences using both a mixed effects linear model and a bootstrap procedure (see Statistical analysis section).

To visualize the spatial network distribution in a 2D plane, we constructed graphs for each condition by binarizing the matrices, establishing the threshold as a number that selected the strongest 1% of connections of each individual matrix. We used the Python library NetworkX version 3.1 with the Kamada-Kawai algorithm (Kamada and Kawai, 1989), a type of force-directed graph that aims to position nodes such that the edges have uniform length and the vertices are uniformly distributed. The nodes corresponding to functional networks whose connectivity changes across conditions were statistically significant were colored using the FN's specific color, while the rest were colored gray to avoid visual crowding.

To examine differences in network topology between Baseline and the rest of the conditions, we computed binary global efficiency for each session. Each weighted matrix was converted to an unweighted

adjacency matrix by retaining only the top 5% strongest connections, to ensure comparable network density across sessions and conditions. Efficiency was then computed on these binarized graphs for all sessions and conditions. To statistically compare the two conditions, we used a Mann-Whitney U test.

We performed a seed-based connectivity analysis restricted to the ROIs that showed significant modulation in the previous analysis, grouped into four networks: two with decreased connectivity in the NOC state (VIS, SMD) and two with increased connectivity (FP, SN). For each participant and condition, we extracted the ROI time series and computed voxelwise connectivity maps using Pearson correlation, followed by Fisher z-transformation. For each network, the resulting z-maps from all its ROIs were averaged at the participant level to obtain a single connectivity map representing that network's whole-brain coupling pattern.

2.6. Entropy and complexity

The statistical complexity and permutation entropy (Bandt and Pompe, 2002) were calculated using the "ordpy" Python library (Pessa and Ribeiro, 2021). We applied the calculation over the BOLD time series of each subject, condition and ROI, using an embedding dimension of d=3 and an embedding delay of tau=1, meaning that each symbol in the symbolic encoding was formed by considering three consecutive samples from the time series. We also evaluated alternative embedding parameters, including embedding dimensions of 2 and 4 and embedding delays of 1, 2, and 3. The analysis was performed both at the level of individual sessions and on time series obtained by concatenating all sessions within each condition. To compare between AVP's and control's entropy and complexity values we employed a bootstrap procedure (see Section 2.7. Statistical analysis).

2.7. Statistical analysis

We applied mixed effects linear models implemented with the Python library Statsmodels, version 0.14.0. All reported p-values were corrected for multiple comparisons using a False Discovery Rate (FDR) correction with a 5% significance level, unless stated otherwise. For the inter-network and intra-network correlation models, we used the following formulas

$$Ic \sim Network + Condition - 1 + (1|Session)$$

$$Ec \sim Network + Condition - 1 + (1|Session)$$

where 'Ic' ('Ecv) is the difference in intra-correlation (inter-correlation) between matrices from a given condition and the Baseline, 'Network' is a categorical variable encoding the network identity (1 to 13), and 'Condition' encodes the four experimental conditions: Baseline (BL), Transition (TR), NOC, and Residual (RES). 'Session' is a random effect variable representing the session number (1 to 20).

For the standard deviation and the CV we employed the models:

$$CV \sim Condition + (1|Session)$$

$$STD \sim Condition + (1|Session)$$

STD stands for standard deviation across correlation values from a single connectivity matrix. The conditions were compared to the Baseline (as we included the intercept) to observe differences in CV relative to the Baseline condition.

For the permutation entropy and statistical complexity we used the following models:$PE \sim Network + Condition - 1 + (1|Session)$

$$SC \sim Network + Condition - 1 + (1|Session)$$

where PE is permutation entropy and SC is statistical complexity.

In order to select significant networks in Fig. S4a we used the model:

$$C \sim Network - 1 + (1|Session)$$

where C is the difference in connectivity between each condition and Baseline. For the analyses of network connectivity per significant network we employed the following model

$$NC \sim Condition - 1 + (1|Session)$$

where NC is the network connectivity for the significant networks visual, somatosensory dorsal, fronto-parietal, salience Network, and ventral attention. Fig. S4a plots the correlation values per condition for all significant networks.

In the difference in network connectivity analysis (Fig. 4) we conducted three separate models:

$$DT \sim Network\_pair - 1 + (1|Session)$$

$$DN \sim Network\_pair - 1 + (1|Session)$$

$$DR \sim Network\_pair - 1 + (1|Session)$$

where DT represents the difference in network correlation between Transition and Baseline, DN represents the difference between NOC and Baseline, and DR represents the difference between Residual and Baseline. 'Network_pair' is a categorical variable representing the network pair (i.e., the networks i and j involved in each correlation value).

For the ROI connectivity analysis in Fig. 5b we conducted three models:

$$DT \sim ROI - 1 + (1|Session)$$

$$DN \sim ROI - 1 + (1|Session)$$

$$DR \sim ROI - 1 + (1|Session)$$

Statistically significant ROIs were divided into those that increased and those that decreased in connectivity in each condition and were plotted in Fig. 5b.

We also compared AVP data with the control group. We implemented a bootstrapping procedure (Davison and Hinkley, 1997) for each of the four conditions and each measure (Inter, Intra, Variation Coefficient, and Network Pair connectivity). We combined each of the 20 values (one per session) from the AVP group with 10 values from the control group (one per participant). Since the control group had 2 participants with 1 condition where the values were NaNs (due to defects), we filtered out the NaN values and sampled with replacement, in each iteration, until we obtained 20 values for the control group. The difference between the averages of the measures for each group was calculated, and the entire process was repeated 50,000 times to obtain a distribution of differences (referred to as the null distribution). We compared the actual difference from the empirical data with this null distribution: the probability of obtaining the actual difference under the null distribution is the p-value associated with that measure and condition. The p-values were adjusted for multiple comparisons using a FDR correction with a 5% significance level. To compare the ROI-level connectivity between the AVP group and the control group, we identified the significant ROIs in the AVP group, averaged them into a single value per session, and compared these values against the corresponding ROIs in the control group using a bootstrap procedure as described before.

For the parameter exploration in the entropy analysis we followed a similar approach. Concatenation provided longer time series, allowing for more reliable estimates of the underlying symbolic probability distributions and, consequently, of entropy and complexity. However, concatenating sessions removed the possibility of applying statistical models. To address this limitation, we implemented a bootstrap-based procedure. Specifically, we generated 100 surrogate concatenated time series by randomly sampling and stitching together sessions from

both the Baseline and NOC. For each surrogate series, we computed entropy and complexity, thus obtaining a null distribution that we approximated as normal using its mean and standard deviation. We then compared the empirical difference, computed from the actual concatenated Baseline and Alteration series (20 sessions each), against this null distribution to derive a p-value.

For the seeds analysis we compared NOC versus Baseline using voxelwise paired t-tests, applying FDR correction at $q < 0.05$, with a minimum cluster size of 10.

3. Results

3.1. Psychological traits and states phenomenology

The micro-phenomenological interview and session-by-session reports revealed a highly structured and reproducible experiential sequence across the 20 fMRI sessions (Table 1). At the beginning of each session, she entered the scanner in an ordinary mental mode, engaging in everyday thoughts and concrete concerns. From this baseline, she intentionally relaxed by scanning her body, loosening muscles, and allowing herself to feel progressively lighter. The constant sound of the MRI scanner served as a stable anchor "like a mantra" that facilitated attentional focusing rather than distracting her. The Transition phase was effortful, unstable, and required active intention. This phase consistently began with the emergence of violet coloration replacing the dark visual field, followed by the gradual appearance of a yellow-violet hexagonal lattice perceived not as an inner image but as a structured pattern "in the air" surrounding her. She emphasized a distinct sense of "double consciousness": while fully aware of being inside the scanner, she simultaneously felt connected to a broader field of experience characterized by serenity, unity, and reduced fragmentation of time. Bodily sensations during this phase were notably variable: in some sessions she reported tension and instability, whereas in others she experienced marked lightness and a diffuse sense of expansion.

Upon entering the fully developed NOC, the experience stabilized into a vivid visionary mode accompanied by profound calmness, spatial expansion, and attenuated bodily boundaries. She reported an "eternal present," a continuous temporal flow with minimal segmentation. Across sessions, the most stable phenomenological motif was the hexagonal network coupled with rhythmic violet pulses. As the state deepened, lucid dream-like scenes emerged: landscapes, horizons, and interactions with imagined figures felt vividly present. In one session, uncrossing her imagined legs produced a strikingly real bodily sensation despite complete physical immobility. Multisensory modulation was also common, particularly deliberate manipulation of the scanner's pitch and timbre, which she described as stretching or modulating the sound "like gum." In several sessions, she reported cubic grids, labyrinth-like structures, and highly organized geometric patterns resembling sacred geometry.

The Residual phase was triggered by the researcher's entrance into the scanner room and unfolded gradually, aided by intentional movement. Although the visionary imagery dissipated quickly, she often remained in an expanded sensory mode for 30 to 60 minutes afterward, reporting heightened brightness, softened edges, and an extended sense of physical and mental openness.

The phenomenology was remarkably consistent across the 20 sessions. The hexagonal network and violet pulse appeared in every session, and most sessions featured variations of geometric structures, depth distortions, bodily expansion, or dream-like imagery. This reproducibility, together with the detailed micro-phenomenological account, supports the interpretation that AVP's NOC is a stable, voluntarily accessible state with a well-defined experiential structure, suitable for systematic neurophenomenological investigation.

Table 1
Neurophenomenological matrix linking subjective experience with brain network dynamics.

Condition	Subjective experience	Neuroimaging findings
Baseline	• Ordinary mentation. • Full bodily awareness. Stable proprioception. • Intentional relaxation and body scanning. · Scanner sound perceived as steady, neutral background.	• Baseline-range intra/inter-network connectivity. • Low global variability. · High entropy, low complexity.
Transition	• Effortful and unstable shift. Bodily tension. • Hexagonal, honeycomb imagery, dynamic brightness. • After threshold, "Double-consciousness": scanner awareness + emerging unity. · Sense of expansion; altered time.	• Peak global variability (high STD, high CV). • Early inter-network decoupling (VIS→VA/AUD/SMD). • ROI-level decreases (visual, CO, SMD). · • Entropy diminishes, complexity increases.
NOC	• Stable immersive visionary mode. • Vivid geometric imagery: violet grids, fractals, pulses. • Altered embodiment. Proprioceptive attenuation. • Scanner sound treated as mantra. · Serenity, unity, timelessness. Deep stable absorption.	• Strong inter-network decoupling (VIS, SMD, VA). • VIS isolated. • VIS: broad decoupling from auditory, somatomotor, pulvinar, cerebellum. • SMD: decoupling from auditory/language regions. • FP: increased connectivity with PCC/precuneus, mPFC, SMA, temporal multimodal, cerebellum. • SN: increased connectivity with PCC/precuneus, insula, thalamus, early visual. · Entropy lower, complexity highest.
Residual	• Abrupt disruption then slow return. • Persisting perceptual alterations (brightness, soft borders). · Gradual re-entry into ordinary mentation.	• Partial reconnection but still low inter-network connectivity vs Baseline. • VIS/SMD remain partially decoupled. • SN mildly more connected. · Entropy/complexity return to baseline.

3.2. Brain imaging

3.2.1. Global connectivity

Intra-network connectivity decreased significantly compared to Baseline in both the NOC (β = -0.009, SE = 0.004, p = 0.038 FDR corrected) and Residual conditions (β = -0.009, SE = 0.004, p = 0.038 FDR corrected) (Fig. 2a, b), and inter-network connectivity decreased in all three conditions compared to the Baseline (Transition; β = -0.007, SE = 0.002, $p < 0.001$ FDR corrected) (NOC; β = -0.005, SE = 0.002, p = 0.001 FDR corrected) (Residual; β = -0.008, SE = 0.002, $p < 0.001$ FDR corrected) (Fig. 2c). The comparison between AVP's results and those of the control group also revealed significant differences, both for inter-network (Baseline v. Transition; p = 0.002, FDR corrected) (Baseline v. NOC; p = 0.01 FDR corrected) and intra-network connectivity (Baseline v. NOC; p = 0.01 FDR corrected) (Baseline v. Residual; p = 0.01). We found no difference between conditions in the control group (Fig. S2a, left, right) except in the inter connectivity for NOC v. Baseline but with the opposite effect (β = 0.019, SE = 0.008, p = 0.043 FDR corrected) (Fig. S2a, middle).

Intra-network connectivity showed no variations across states, whereas the most robust effects were observed in inter-network connectivity during the Transition (β = -0.295, SE = 0.134, p = 0.04 FDR corrected) and Residual (β = -0.345, SE = 0.134, p = 0.03 FDR corrected) conditions (Fig. 2d). Inter-network connectivity decreased relative to Baseline during Transition and Residual, suggesting a reorganization of the existing networks rather than a dissolution of the networks observed during normal wakefulness. In the control group, the only statistically significant difference was observed between NOC and

Baseline conditions (β = 0.645, SE = 0.264, p = 0.03 FDR corrected), where normalized inter-network connectivity was higher during Baseline than in NOC, an effect opposite to that observed in AVP (Fig. S2b).

Fig. 2e-g shows the plots with intra-network connectivity on the x-axis and inter-network connectivity on the y-axis. The base or starting point of each vector is the intra-inter pair of the Baseline, and the arrowhead or endpoint is the specific pair of the graphed condition. Some networks vary greatly in their connectivity while others change very little, suggesting that the changes associated with AVP's phenomenological states are network-specific. In particular, the visual and somatosensory networks strongly decrease their inter-network connectivity, while frontoparietal network connectivity increases monotonically across conditions (Fig. 2 e-g). In the Transition vs. Baseline comparison, we observed only one functional network that significantly changed: the visual network, which decreased its connectivity (β = -0.025, p < 0.001). In NOC vs. Baseline comparison, three networks significantly decreased their connectivity: the visual network (β = -0.032, p < 0.001), the ventral attention network (β = -0.017, p = 0.048), and the sensorimotor dorsal network (β = -0.024, p = 0.018) and one increased its connectivity: the frontoparietal network (β = 0.018, p = 0.019). In Residual vs. Baseline, the visual network (β = -0.032, p < 0.001), the ventral attention network (β = -0.010, p = 0.013), and the sensorimotor dorsal network (β = -0.035, p < 0.001) all decreased their connectivity, while the salience network (β = 0.018, p = 0.0094) increased its connectivity. In the control group, no significant differences were observed between conditions in either intra- or inter-network connectivity (Fig. S3), and none of the connectivity changes seen in AVP were replicated.

Standard deviation increased significantly specifically in the Transition (Transition v. Baseline; β = -0.009, SE = 0.004 p = 0.03 FDR corrected) and this increment was specific to the Transition (Transition v. NOC, β = -0.008, SE = 0.004 p = 0.047 FDR corrected) (Transition v. Residual, β = -0.011, SE = 0.004 p = 0.013 FDR corrected) (Fig. 2h, top). This shows that the standard deviation values were higher during the Transition compared to Baseline, indicating increased global variability. Comparing AVP to controls, this increment showed no significance (Baseline v. Transition; p = 0.24) (Transition v. NOC; p = 0.07) (Transition v. Residual; p = 0.09). We also found that the coefficient of variation increased significantly in all conditions (Baseline v. Transition; β = 1.823, SE = 0.774, p = 0.018 FDR corrected) (Baseline v. NOC; β = 1.889, SE = 0.774, p = 0.018 FDR corrected), (Baseline v. Residual; β = 2.146, SE = 0.774, p = 0.016 FDR corrected) (Fig. 2h, bottom) and comparing AVP to controls all conditions were close but not significant (Baseline v. Transition; p = 0.055) (Baseline v. NOC; p = 0.055) (Baseline v. Residual; p = 0.055).

3.2.2. Entropy and complexity

The entropy analysis showed significantly lower values in the Transition compared to Baseline (β = -0.0129, SE = 0.0003, p < 0.001, FDR corrected) and to NOC (β = -0.0169, SE = 0.0003, p < 0.001, FDR corrected) (Fig. 3a). Similarly, statistical complexity also exhibited a significantly higher value in Transition (β = 0.0010, SE = 0.0002, p < 0.001, FDR corrected) and NOC (β = 0.0013, SE = 0.0002, p < 0.001, FDR corrected) as compared to Baseline (Fig. 3b). In contrast, no statistically significant differences were observed between the Baseline and Residual for either entropy or complexity. The entropy-complexity plane (Fig. 3c) provides a clear visualization of the dynamic shifts in brain activity across conditions. We found significant differences between AVP and the control group only in the Baseline vs. Residual conditions for both entropy (p = 0.008, FDR corrected) and complexity (p = 0.016, FDR corrected). When we varied the embedding parameters away from the canonical configuration (d = 3, tau = 1), we found no statistically significant differences between Baseline and NOC (Fig. S5). Concatenating all sessions into a single timeseries for each condition (Fig. S6) we observed statistically significant differences between Baseline and NOC for all combinations of embedding dimension and delay (d=2, tau=1, p < 0.001; d=4, tau=1; p < 0.001; d=3, tau=2, p < 0.001; d=3, tau=3, p < 0.001).

3.2.3. Network-level analyses

Focusing on the five networks that showed significant effects (visual, somatosensory dorsal, ventral attention, fronto-parietal, and salience), we observed network-specific connectivity changes across conditions in AVP (Fig. S4a), with the visual and somatosensory dorsal networks consistently showing decreased connectivity, and the fronto-parietal network showing increased connectivity during the NOC state. Comparisons with controls confirmed that these effects were specific to AVP (Fig. S4b). Complete statistics are reported in the Supplementary Material.

We found that several connections changed during Transition, NOC, and Residual (Fig. 4). The overall picture shows that the visual network appears to alter its connections the most, particularly with the ventral attention, auditory, and sensorimotor networks (i.e., the sensory and attentional networks) (see Table S3 for the complete list of network pairs). In the control group, no significant differences were found between conditions (see Table S4 for the complete list of network pairs).

3.2.4. ROI-level analyses

NOC state significantly differed from Baseline in network efficiency (U = 126, p = 0.046) with NOC showing higher values (mean efficiency = 0.344) than Baseline (mean efficiency = 0.335). However, we did not find significant differences between Baseline and Transition (U = 244, p

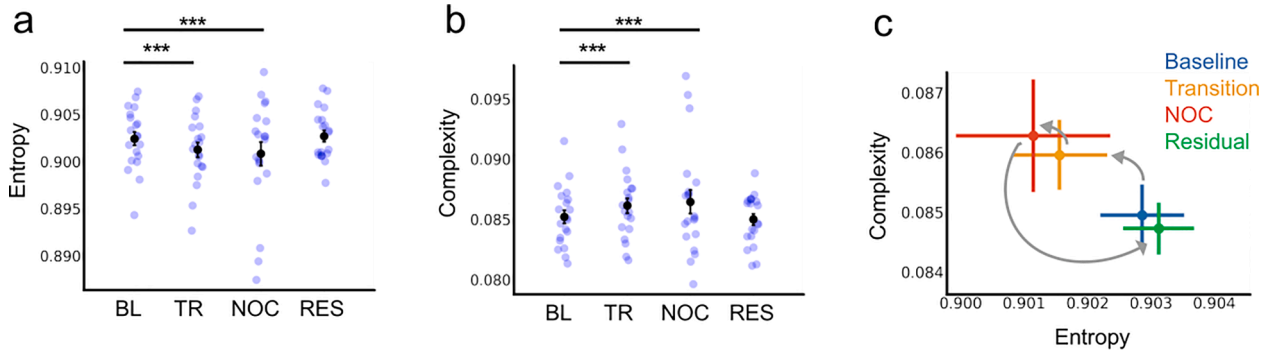

Fig. 3. Permutation entropy and Statistical complexity. a) The entropy shows significant differences between Baseline and Transition, and Baseline and NOC, but no difference between Baseline and Residual. b) The complexity shows a similar behavior with differences between Baseline and Transition, and Baseline and NOC but no difference between Baseline and Residual. A triple asterisk indicates p < 0.001. c) Entropy-Complexity plane. Initially, Baseline starts with high entropy and low complexity. As it progresses to Transition and NOC, the entropy decreases and complexity increases. Finally, the condition Residual returns to similar levels of entropy and complexity as Baseline. The bars denote standard error of the mean.

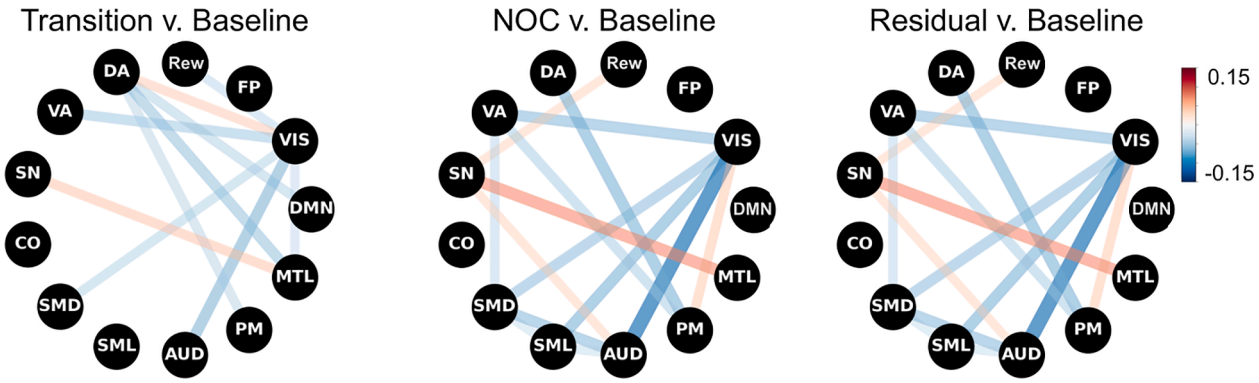

Fig. 4. Network-level connectivity changes. Difference in inter-network connectivity for each condition compared to baseline. Asterisks indicate significance in the linear mixed model (FDR corrected); see Table S3 for a complete list of significant network pairs. Blue lines signify a decrease relative to baseline, while red lines indicate an increase. DA = Dorsal Attention; MTL = Medial Temporal Lobe; DMN = Default Mode Network; Rew = Reward; SN = Salience Network; FP = Frontoparietal; SMD = Somatomotor Dorsal; SML = Somatomotor Lateral; VA = Ventral Attention; CO = Cingulo-Opercular; VIS = Visual; AUD = Auditive; PM = Parieto-medial.

= 0.24) or between Baseline and Residual (U = 139, p = 0.10). When comparing the conditions within the control group we found no statistically significant differences between Baseline and the rest of the conditions (Baseline vs. Transition: U = 61, p = 0.42; Baseline vs. NOC: U = 55, p = 0.73; Baseline vs. Residual: U = 85, p = 0.53). ROI-level analyses (Fig. 5b; Table S5) showed no increases in connectivity during Transition, but several decreases, particularly in visual, cingulo-opercular, and sensorimotor areas. This disconnection pattern intensified in the NOC state and extended to dorsal and ventral attention ROIs, while a subset of frontoparietal ROIs showed increased connectivity. No significant connectivity differences across conditions were found in the control group. Compared to the control group, AVP showed significantly different ROI-level connectivity patterns during Transition (decreased connectivity, p = 0.03, FDR-corrected) and NOC conditions (both increases and decreases, p = 0.03, FDR-corrected, for each). No significant differences were observed in the Residual condition.

Seed-based connectivity of the visual network during the NOC state showed large-scale decreases relative to Baseline (Fig. 6a). We found reduced coupling with bilateral temporal cortex (superior and middle temporal gyri, including Heschl's gyrus and opercular regions), postcentral and precentral sensorimotor cortices, inferior orbitofrontal cortex, limbic–parahippocampal regions, the thalamus (pulvinar and posterior nuclei), and extensive portions of the posterior cerebellum. No voxel showed increased connectivity at statistical threshold. A complete

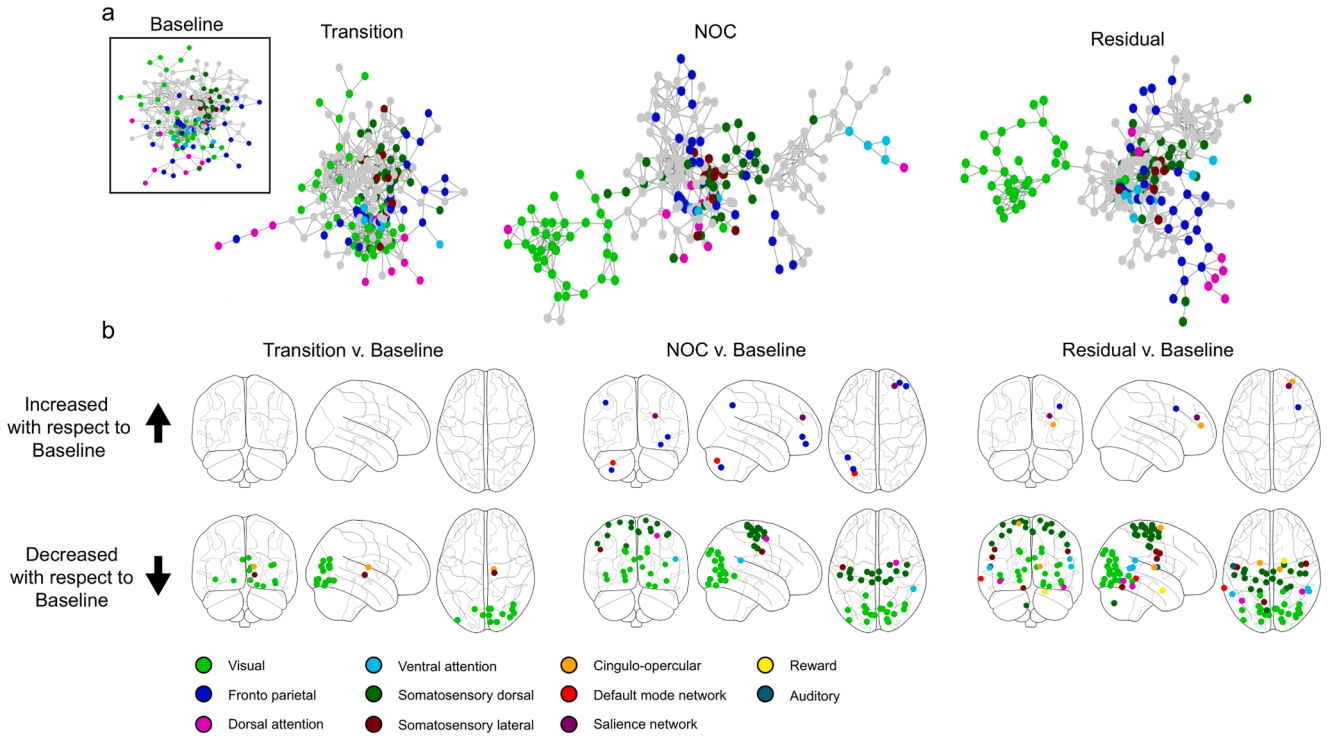

Fig. 5. ROI-based connectivity. a) Topology of AVP connectivity: minimal energy plots of the average networks for all conditions. It is notable how the visual network becomes isolated from the rest in the NOC and Residual conditions compared to Baseline. b) Glass brain visualizations showing regions of interest (ROIs) with significant changes in connectivity for each experimental condition relative to baseline after correction. Each panel corresponds to one comparison: Transition vs. Baseline, NOC vs. Baseline, and Residual vs. Baseline. ROIs displayed in the upper half of each brain showed increased connectivity relative to baseline, while those in the lower half showed decreased connectivity. Note that significance is assessed at the ROI level, independent of network identity; thus, the prominence of a given color reflects the network associated with that particular ROI. See Table S5 for the full list of significant network pairs.

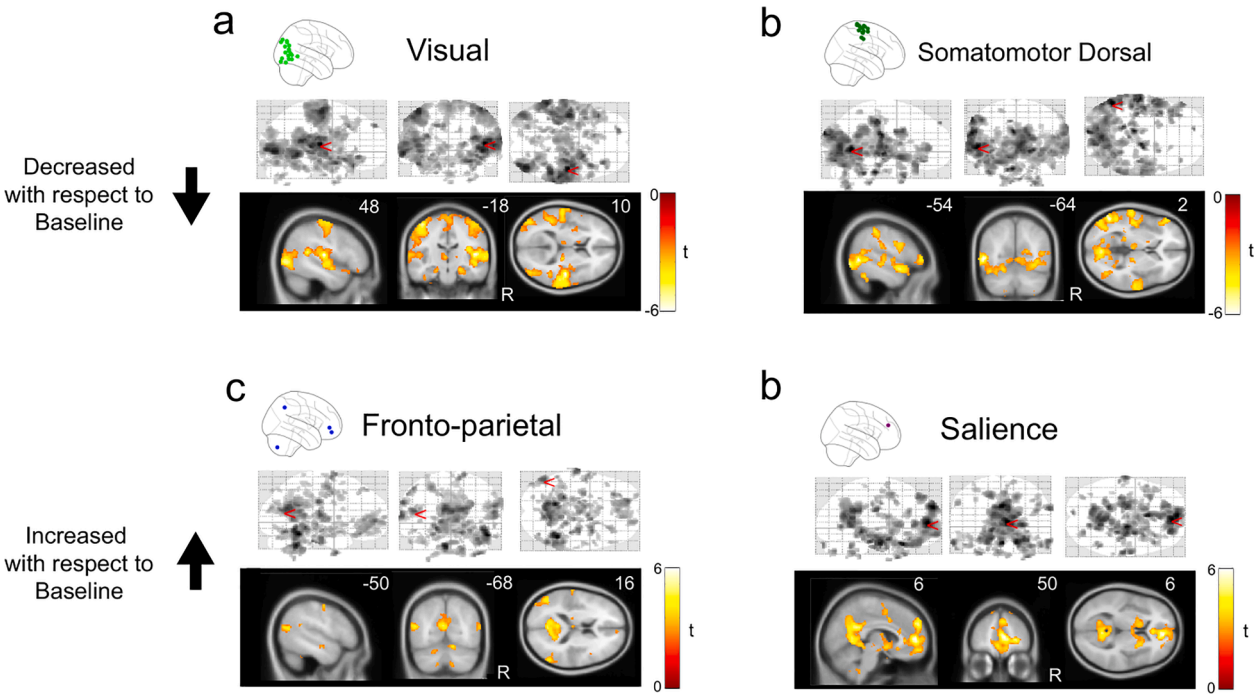

Fig. 6. Network-level Seed-Based Connectivity Analysis. Seed-based functional connectivity analysis using significant ROIs from Fig. 5 within four large-scale networks: visual (a), dorsal somatomotor (b), frontoparietal (c), and salience (d). For each network, connectivity maps were computed for each ROI and subsequently averaged to obtain a network-level correlation map. Statistical significance was assessed using FDR correction at 0.05, and only surviving voxels are displayed.

report of significant clusters can be found in Table S6.

The SMD network showed a similar pattern of disconnection during NOC (Fig. 6b). We found decrements in connectivity with bilateral auditory and language cortices, including superior and middle temporal gyri, Heschl's gyrus, the planum temporale, Rolandic operculum, insula, and inferior frontal gyrus, indicating a general decoupling between SMD and the language network, among other regions. No voxel showed increased connectivity at statistical threshold. A complete report of significant clusters can be found in Table S7.

FP connectivity conversely increased, in agreement with our previous analyses (Fig. 6c). We found increased connectivity with precuneus and posterior cingulate, bilateral middle and inferior temporal cortices, precentral and supplementary motor regions, medial prefrontal cortex, and extensive portions of the posterior cerebellum. No voxel showed decreased connectivity at statistical threshold. A complete report of significant clusters can be found in Table S8.

SN also increases its connectivity (Fig. 6d), particularly with precuneus/posterior cingulate, lingual and calcarine cortex, anterior cingulate, bilateral basal ganglia, thalamus, and posterior cerebellum, indicates a broad strengthening with regions involved in internal monitoring and multisensory integration. No voxel showed decreased connectivity at statistical threshold. A complete report of significant clusters can be found in Table S9.

4. Discussion

4.1. Summary of main findings

In this study, we examined the neurophenomenology of a self-induced NOC by integrating first-person reports with repeated measures of brain activity. Unlike most empirical approaches based on pharmacological manipulations or pathological conditions, this non-pharmacological and volitionally induced a structured, reproducible sequence of experiential phases while preserving full awareness. This design enabled a detailed examination of how systematic changes in experience correspond to large-scale neural dynamics across 20 independent sessions. Our analytic framework was guided by four hypotheses derived from research on psychedelic, meditative, and hypnotic states (Cardeña et al., 2013; Carhart-Harris et al., 2012; Dor-Ziderman et al., 2016; Gosseries et al., 2024; Lanfranco et al., 2021; Lewis-Healey et al., 2024; Mainieri et al., 2017; Smigielski et al., 2019; Stoliker et al., 2024; Tagliazucchi et al., 2016; Timmermann et al., 2023). Below, we discuss each hypothesis in relation to the present findings.

4.2. Evaluation of the four hypotheses

Hypothesis 1 predicted reduced inter-network connectivity during NOC. This prediction was strongly supported: dorsal somatomotor, visual, and ventral attention networks showed pronounced decoupling relative to Baseline. In the control group, the modest but significant increase in inter-network connectivity observed in the NOC condition likely reflects non-specific fluctuations in vigilance or spontaneous imagery rather than a structured state change, consistent with prior reports of transient increases in large-scale correlations during relaxed wakefulness and early drowsiness (Tagliazucchi and van Someren, 2017).

AVPs reduced inter-network visual connectivity during NOC resonates with her intense and highly structured visual phenomena, including a recurring yellow hexagonal grid, violet pulses, and fractal-like imagery. Such geometric imagery has been described in entoptic and drug-induced visual research (Miyashita, 1995; Siegel, 1977; Siegel and Jarvik, 1975), and computational models suggest that these lattice-like percepts arise from intrinsic excitatory and inhibitory interactions in early visual cortex when sensory input is reduced and cortical excitability increases (Bressloff et al., 2001, 2002; Ermentrout and Cowan, 1979). Also, the pronounced decoupling of somatomotor and ventral attention networks indicates a functional disengagement from external sensory input and bodily orientation, consistent with AVP's descriptions of reduced boundaries and immersive visual absorption. Reduced recruitment of the ventral attention network, which normally detects external salience and reorients attention, likely reflects

a shift toward internally maintained imagery, while somatomotor decoupling aligns with attenuation of proprioception and affected body perception. Together, these results point to a reorganization of large-scale functional architecture that favors internally driven and symbolically rich experiential content.

The visual seed showed that the visual network became more segregated during the NOC state, with reduced connectivity to sensorimotor, auditory, orbitofrontal, and thalamic regions. This pattern matches the participant's reports of vivid internal imagery, diminished orientation to external input, and a weaker sense of bodily and auditory anchoring. The decreases in visuo-auditory and visuo-sensorimotor coupling, together with the disconnection from posterior cerebellum and pulvinar, fit well with accounts of "closed-loop" visual cortex dynamics and with models in which geometric imagery arises from intrinsic self-organization within early visual areas. These results indicate a shift toward predominantly endogenous visual processing, consistent with observations from psychedelic research where visual regions become more autonomous and internally driven (Carhart-Harris et al., 2016; Huels et al., 2021; Roseman et al., 2018) and with reports of sensory down-weighting in deep meditative absorption (Ganesan et al., 2024; Yang et al., 2023).

The SMD seed analysis showed a clear decoupling from auditory and language-related cortices, including bilateral STG/MTG, Heschl's gyrus, opercular regions, and inferior frontal gyrus. This large-scale disengagement suggests a temporary suspension of the audio-motor loop that normally supports speech, verbal imagery, and auditory prediction. The finding is consistent with the participant's reduced internal dialogue, altered sense of bodily anchoring, and voluntary modulation of scanner sounds.

Hypothesis 2 predicted increased connectivity within frontoparietal and default mode networks. This hypothesis was partially supported. We found a significant increase in FP connectivity during the NOC, which returned to baseline during recovery. This pattern is consistent with AVP's descriptions of heightened awareness, cognitive clarity, and intentional engagement with inner experience. The salience network also showed early and sustained increases, particularly in the dACC, thalamus, and insula, which may reflect enhanced interoceptive and attentional regulation (Quigley et al., 2021; Salomon et al., 2016; Tsakiris and Critchley, 2016). However, DMN connectivity did not show significant changes, diverging from prior findings in psychedelic research (Gattuso et al., 2023), which reported decreases in within-DMN and increases in DMN-inter-network connectivity. Consistent with this distinction, our seed analysis revealed no increases within the DMN itself, but showed clear cross-network strengthening between FP and posterior midline DMN hubs (precuneus/posterior cingulate) during NOC. This difference likely reflects the distinct nature of the two states: psychedelic experiences are pharmacologically induced and often associated with profound ego dissolution, whereas AVP's state was self-induced and stable. Similar patterns have been reported in non-pharmacological NOC such as shamanic trance, auto-induced cognitive trance, and deep absorption, where vivid imagery and sensory attenuation occur without disintegration of the DMN or loss of self (Grégoire et al., 2024; Hove et al., 2016; Huels et al., 2021; Yang et al., 2023). These characteristics may sustain a balanced engagement of self-referential and control processes, preventing the DMN disintegration typically observed under psychedelics. Thus, rather than a collapse or hyperintegration of the DMN, AVP's state may involve a dynamic reorganization that preserves introspective awareness within a stable network architecture, supported by selective increases in FP–DMN coupling rather than global DMN modulation.

The frontoparietal seed showed increased connectivity with the precuneus/posterior cingulate, medial prefrontal cortex, temporal multimodal regions, precentral/SMA areas, and posterior cerebellum. This configuration corresponds to a network known to support internally focused attention, scene construction, visuospatial imagery, and sensorimotor prediction. The strengthening of FP-precuneus coupling is particularly notable, as similar patterns have been observed in states of sustained internal absorption (Hasenkamp et al., 2012) and in high-field intensive-sampling meditation studies demonstrating enhanced FP-midline integration during deep concentration (Yang et al., 2023). This aligns closely with the participant's descriptions of vivid internal scenes, stable inward-directed focus, and the feeling of "being inside" a visual environment (Grégoire et al., 2024; Huels et al., 2021).

Finally, the salience network showed increased connectivity during the NOC state, especially with the precuneus/posterior cingulate, lingual and calcarine cortex, anterior cingulate, basal ganglia, thalamus, and cerebellar Crus. This pattern suggests enhanced interoceptive monitoring, subcortical regulation, and integration of internally generated visual and mnemonic content. The coupling with posterior midline and early visual regions is consistent with the participant's geometric imagery, depth sensations, and sustained inward attention. Similar salience-driven stabilization of internally oriented states has been reported in shamanic trance, auto-induced cognitive trance, and states of deep meditative absorption (Gosseries et al., 2024; Hove et al., 2016; Mainieri et al., 2017).

Hypothesis 3 predicted increased variability during the Transition. The data strongly supported this prediction, as we observed a marked increase in the variability of functional connectivity, both in absolute terms and relative to the mean. This heightened variability was especially prominent in the salience and frontoparietal networks, and diminished once the NOC stabilized. AVP described this phase as effortful and disorganized, involving bodily tension, active searching, and a sense of cognitive turbulence. Once she crossed a self-identified threshold that marked the entry into the NOC this tension dissolves, giving way to a stable and effortless experiential mode in which she reports being able to remain indefinitely, as she does in her everyday life. These findings align with Tart's (1976) proposal that transitions into NOC states involve temporary disorganization followed by the emergence of a new experiential order. They also support recent models emphasizing increased network flexibility and metastability as markers of non-ordinary states (Cabral et al., 2022; Cavanna et al., 2018; Tagliazucchi and van Someren, 2017), suggesting that transient neural destabilization may be a necessary condition for accessing alternate modes of conscious experience.

Unexpectedly, although entropy and complexity depend only on the ordinal structure of the BOLD signal rather than its amplitude, they also exhibited substantial variability across sessions. This pattern likely reflects the combined influence of two factors. First, the relatively short duration of each block (150 volumes) makes entropy and complexity estimates less stable across runs. Second, and more importantly, while the participant reported a consistent experiential core, she also described subtle variations in depth, vividness, and immersion across sessions. These fine-grained phenomenological fluctuations may be captured more directly by entropy and complexity-based metrics than by connectivity measures, which integrate over slower timescales. In line with this interpretation, entropy and complexity were also the only measures that fully returned to baseline during the Residual phase, suggesting that they are particularly sensitive to the stabilization and dissolution of the NOC.

Hypothesis 4 predicted systematic entropy and complexity changes. This was confirmed: we observed decreased entropy and increased statistical complexity during both Transition and NOC compared to Baseline, indicating a shift toward neural dynamics that are more structured yet less stochastic. These changes reversed in the Residual phase, suggesting that the brain's information-processing architecture flexibly reconfigures in response to the NOC and can return to its Baseline organization even though AVP continued to experience a residual form of the state. Notably, entropy and complexity were the only measures that fully returned to baseline levels during Residual, underscoring their sensitivity to the stabilization and subsequent dissolution of the NOC.

From a theoretical perspective, these findings suggest that the observed decrease in entropy and increase in complexity may reflect a

transient relaxation of stable network configurations, allowing new patterns of conscious content to emerge. Such temporary reorganizations could represent a flexible rebalancing between top-down constraints and bottom-up dynamics, supporting the emergence of novel experiential structures. In this view, increased complexity reflects the emergence of richly differentiated patterns of brain activity, while reduced entropy suggests a departure from the high-noise regime of unconstrained cognition toward a metastable, self-organizing mode (Cavanna et al., 2018; Coppola et al., 2022; Mateos et al., 2018; Mindlin et al., 2024). This entropic trajectory may support the phenomenological qualities reported by AVP, such as enhanced insight, symbolic integration, and the dissolution of conventional perceptual and temporal boundaries.

4.3. Convergences with meditation, trance, and psychedelic research

Research on trance and related non-ordinary states provides convergent evidence for structured reorganization of large-scale networks. fMRI and EEG studies of shamanic and mediumistic trance (Hove et al., 2016; Huels et al., 2021; Mainieri et al., 2017) consistently report increased coupling among hubs of the default mode and control networks, particularly PCC, dACC, and insula, together with reduced connectivity in sensory pathways such as auditory cortex. This pattern reflects a shift toward amplified internally oriented processing and partial decoupling from exteroception. A comparable configuration appears in AVP's NOC state, where visual, somatosensory, and ventral attention networks showed marked disconnection, while frontoparietal and salience networks strengthened (Rogerson et al., 2021). Phenomenological reports from auto-induced cognitive trance (AICT) and Mahorikatan practices (Grégoire et al., 2024; Oswald et al., 2025; Vanhaudenhuyse et al., 2024) describe vivid imagery, proprioceptive alterations, absorption, and narrowed external orientation-features that partially overlap with AVP's experience. Trance studies repeatedly highlight a pattern of sensory attenuation together with intensification of internally generated experience, a combination that provides a strong external validation for the network configuration observed in our data. Also, Studies of deep absorption (Ganesan et al., 2024; Yang et al., 2023) show highly reliable within-subject modulation of sensory cortices, attentional hubs, and subcortical structures. These convergences suggest that sensory attenuation and heightened internal integration may represent general organizational motifs across non-pharmacological NOC, even when their induction methods and cultural contexts differ.

Together with trance and meditation research, these findings converge on a growing view that non-pharmacological NOC states are characterized by coherent yet reorganized network architectures, combining sensory decoupling with strengthened control and salience engagement, and exhibiting stable within-subject trajectories over time. This situates AVP's case within a broader class of intentional NOC that share both phenomenological structure and reproducible neural dynamics.

4.4. Linking networks changes and AVP reports

Table 1 summarizes the four experimental phases by aligning AVP's subjective reports with the corresponding large-scale network patterns. Baseline is characterized by ordinary mentation, intact bodily awareness, and a stable sensory frame, accompanied by typical intra- and inter-network connectivity, low variability, and high-entropy/low-complexity dynamics. During the Transition, AVP reports bodily tension, unstable attention, and the first appearance of geometric imagery in the form of honeycombs and violet pulses of light; this phase matches a peak in global variability (high STD and CV), early network decoupling especially in visual, cingulo-opercular, and somatomotor-dorsal regions, and a drop in entropy coupled with an increase in complexity. The NOC state corresponds to a stable, effortless immersive mode with vivid internal imagery, reduced proprioceptive grounding, and sustained inward focus; neurally, this aligns with strong inter-network decoupling in VIS, SMD, and VA, isolation of the visual system, disengagement of language network from SMD and increased FP and SN coupling with posterior midline and sensory hubs such as PCC/posterior cingulate, together with the lowest entropy and highest complexity. Finally, the Residual phase combines partial return to ordinary mentation with lingering perceptual and bodily alterations, mirrored by partial reconnection of networks, persistent reductions in inter-network connectivity (mainly VIS, VA, SMD), and a full return of entropy and complexity to baseline levels.

It is worth noting that AVP presents lifelong synesthetic traits, characterized by consistent cross-modal associations between sensory and affective modalities. Rather than confounding the present findings, this feature may help contextualize them. Synesthesia reflects a stable neurocognitive organization marked by increased structural and functional coupling across sensory association areas-patterns that may facilitate the emergence of vivid, multimodal imagery and fluid perceptual integration during non-ordinary states. In this light, AVP's synesthetic predisposition could have amplified the integrative and high-entropy dynamics observed in the visionary condition, offering a natural model of how enduring neural architectures interact with transient reorganizations of consciousness.

4.5. Limitations

This study has several limitations. First, the proposed experiential stages remain coarse approximations. Although they capture major transitions, more granular tracking, such as real-time experience sampling, would improve temporal resolution and allow finer alignment between subjective reports and neural changes (Stawarczyk et al., 2011). Moreover, not all sessions were phenomenologically identical; subtle variations across NOC states could be better captured by increasing the number of sessions and examining recurring experiential features in more detail—for instance, identifying neural correlates of the reported out-of-body experiences. Second, only a single formal micro-phenomenological interview was conducted, despite AVP undergoing 20 sessions. However, this was complemented by detailed self-reports after each session, which showed strong consistency with the interview and support the reproducibility of the experiential pattern across sessions. While these reports allowed us to interpret certain neural changes in light of recurring experiential features, we acknowledge that these interpretations are experience-informed inferences, not formally tested correlations. This limits the strength of claims linking specific phenomenological content to particular network-level dynamics. Third, control participants did not provide structured post-scan interviews. However, all were asked open-ended questions after scanning, following standard resting-state protocols to ensure they had not fallen asleep or entered unintended mental states. All reported typical mentation, such as imagining everyday scenes or recalling recent events. Fourth, the exclusive use of fMRI limits temporal precision and may overlook fast neural transitions. Future studies could incorporate EEG or MEG to capture rapid shifts, particularly during threshold-crossing events, which AVP describes as nearly instantaneous. These additions would enable a more temporally resolved understanding of the dynamics underlying voluntary NOC induction. Finally, as this is an in-depth single-case study, the findings are not statistically generalizable to the wider population. AVP's ability to reliably and volitionally induce a specific NOC, while maintaining a clear and continuous sense of self and full awareness of the context, is rare and may not represent typical NOC experiences. Our interpretations are constrained by the uniqueness of her profile and the absence of replication in other individuals. Rather than offering generalizable conclusions, this study aims to generate hypotheses, demonstrate methodological possibilities, and contribute conceptually to the neurophenomenology of consciousness. The case demonstrates how subjective and neural data can be integrated to study complex experiential states in detail, but further work across diverse

participants and contexts is needed to establish broader principles. We hope this work encourages both caution in extrapolation and curiosity about the heterogeneity of NOC experiences.

4.6. Conclusions

This study demonstrates how a self-induced NOC can be characterized as a coherent yet reorganized mode of conscious experience, with reproducible large-scale signatures tightly aligned with a phenomenological sequence. It highlights the value of integrating first-person reports with network-based neuroimaging and suggests that volitional modulation of consciousness may reveal general principles of brain dynamics across diminished and expanded states of awareness.

Data and code availability

Data not publically available but it can be shared upon reasonable request.

The code used to analyze the data and generate the results is available at https://github.com/dellabellagabriel/visionary-state. For further inquiries, please contact the corresponding authors

CRediT authorship contribution statement

Gabriel Della Bella: Writing – review & editing, Writing – original draft, Visualization, Validation, Software, Methodology, Investigation, Formal analysis, Data curation, Conceptualization. **Agustina Velez Picatto:** Writing – review & editing, Writing – original draft, Visualization, Validation, Software, Methodology, Investigation, Formal analysis, Data curation, Conceptualization. **Dante Sebastián Galván Rial:** Writing – review & editing, Writing – original draft, Software, Resources, Methodology, Data curation. **Sebastián Cukier:** Writing – review & editing, Writing – original draft, Investigation. **Gustavo Foa Torres:** Writing – review & editing, Writing – original draft, Resources, Investigation. **Magaly Catanzariti:** Writing – review & editing, Writing – original draft, Software, Investigation. **Diego Mateos:** Writing – review & editing, Writing – original draft, Software, Methodology, Investigation, Formal analysis. **Pedro Lamberti:** Writing – review & editing, Writing – original draft, Visualization, Validation, Supervision, Software, Resources, Methodology, Investigation, Formal analysis, Data curation, Conceptualization. **Etzel Cardeña:** Writing – review & editing, Writing – original draft, Visualization, Validation, Supervision, Software, Resources, Methodology, Investigation, Formal analysis, Data curation, Conceptualization. **Pablo Barttfeld:** Writing – review & editing, Writing – original draft, Visualization, Validation, Supervision, Software, Resources, Methodology, Investigation, Formal analysis, Data curation, Conceptualization.

Declaration of competing interest

There are no conflicts of interest.

Acknowledgements

This research was supported by Agencia Nacional de Promoción Científica y Tecnológica, Argentina (Grants #2018-03614 and CAT-I-00083). We thank the three anonymous reviewers and the Guest Editors for their constructive feedback and thoughtful suggestions, which significantly improved the clarity and scope of the manuscript. The authors used ChatGPT to assist with English grammar editing. All scientific content, analyses, and interpretations were written, reviewed, and approved by the authors.

Supplementary materials

Supplementary material associated with this article can be found, in the online version, at doi:10.1016/j.neuroimage.2026.121784.

References

Bandt, C., Pompe, B., 2002. Permutation entropy: A natural complexity measure for time series. Phys. Rev. Lett. 88 (17), 174102. https://doi.org/10.1103/PhysRevLett.88.174102.

Barttfeld, P., Bekinschtein, T.A., Salles, A., Stamatakis, E.A., Adapa, R., Menon, D.K., Sigman, M., 2015. Factoring the brain signatures of anesthesia concentration and level of arousal across individuals. NeuroImage: Clin. 9, 385–391. https://doi.org/10.1016/j.nicl.2015.08.013.

Berkovich-Ohana, A., 2015. A case study of a meditation-induced altered state: increased overall gamma synchronization. Phenomenol. Cogn. Sci. 1 (16), 91–106. https://doi.org/10.1007/s11097-015-9435-x.

Bressloff, P.C., Cowan, J.D., Golubitsky, M., Thomas, P.J., Wiener, M.C., 2001. Geometric visual hallucinations, euclidean symmetry and the functional architecture of striate cortex. Philos. Trans. R. Soc. Lond. B: Biol. Sci. 356 (1407), 299–330. https://doi.org/10.1098/rstb.2000.0769.

Bressloff, P.C., Cowan, J.D., Golubitsky, M., Thomas, P.J., Wiener, M.C., 2002. What geometric visual hallucinations tell us about the visual cortex. Neural Comput. 14 (3), 473–491. https://doi.org/10.1162/089976602317250861.

Cabral, J., Castaldo, F., Vohryzek, J., Litvak, V., Bick, C., Lambiotte, R., Friston, K., Kringelbach, M.L., Deco, G., 2022. *Synchronization in the connectome: metastable oscillatory modes emerge from interactions in the brain spacetime network* [Preprint]. Neuroscience. https://doi.org/10.1101/2022.01.06.475196.

Cardeña, E., 2005. THE PHENOMENOLOGY OF DEEP HYPNOSIS: QUiescent and physically active. Int. J. Clin. Exp. Hypn. 53 (1), 37–59. https://doi.org/10.1080/00207140490914234.

Cardeña, E., Berkovich-Ohana, A., Valli, K., Barttfeld, P., Gomez-Marin, A., Greyson, B., Kumar, V.K., Laureys, S., Luhrmann, T.M., Newberg, A., Preller, K.H., Putnam, F.W., Tagliazucchi, E., Walsh, R., Carter, O., Yaden, D., 2025. A consensus taxonomy of altered (nonordinary) states of consciousness: bringing order to disarray. Psychol. Conscious.: Theory Res. Pract. https://doi.org/10.1037/cns0000431.

Cardeña, E., Jönsson, P., Terhune, D.B., Marcusson-Clavertz, D., 2013. The neurophenomenology of neutral hypnosis. Cortex 49 (2), 375–385. https://doi.org/10.1016/j.cortex.2012.04.001.

Carhart-Harris, R.L., Erritzoe, D., Williams, T., Stone, J.M., Reed, L.J., Colasanti, A., Tyacke, R.J., Leech, R., Malizia, A.L., Murphy, K., Hobden, P., Evans, J., Feilding, A., Wise, R.G., Nutt, D.J., 2012. Neural correlates of the psychedelic state as determined by fMRI studies with psilocybin. Proc. Natl. Acad. Sci. 109 (6), 2138–2143. https://doi.org/10.1073/pnas.1119598109.

Carhart-Harris, R.L., Muthukumaraswamy, S., Roseman, L., Kaelen, M., Droog, W., Murphy, K., Tagliazucchi, E., Schenberg, E.E., Nest, T., Orban, C., Leech, R., Williams, L.T., Williams, T.M., Bolstridge, M., Sessa, B., McGonigle, J., Sereno, M.I., Nichols, D., Hellyer, P.J., Nutt, D.J., 2016. Neural correlates of the LSD experience revealed by multimodal neuroimaging. Proc. Natl. Acad. Sci. 113 (17), 4853–4858. https://doi.org/10.1073/pnas.1518377113.

Cavanna, F., Vilas, M.G., Palmucci, M., Tagliazucchi, E., 2018. Dynamic functional connectivity and brain metastability during altered states of consciousness. Neuroimage 180, 383–395. https://doi.org/10.1016/j.neuroimage.2017.09.065.

Chennu, S., O'Connor, S., Adapa, R., Menon, D.K., Bekinschtein, T.A., 2016. Brain connectivity dissociates responsiveness from drug exposure during Propofol-induced transitions of consciousness. PLoS Comput. Biol. 12 (1), e1004669. https://doi.org/10.1371/journal.pcbi.1004669.

Coppola, P., Allanson, J., Naci, L., Adapa, R., Finoia, P., Williams, G.B., Pickard, J.D., Owen, A.M., Menon, D.K., Stamatakis, E.A., 2022. The complexity of the stream of consciousness. Commun. Biol. 5 (1), 1173. https://doi.org/10.1038/s42003-022-04109-x.

Davison, A., Hinkley, D., 1997. Bootstrap methods and their application. J. Am. Stat. Assoc. 94. https://doi.org/10.2307/1271471.

Deeley, Q., Walsh, E., Oakley, D.A., Bell, V., Koppel, C., Mehta, M.A., Halligan, P.W., 2013. Using hypnotic suggestion to model loss of control and awareness of movements: an exploratory fMRI study. PLoS. One 8 (10), e78324. https://doi.org/10.1371/journal.pone.0078324.

Dor-Ziderman, Y., Ataria, Y., Fulder, S., Goldstein, A., Berkovich-Ohana, A., 2016. Self-specific processing in the meditating brain: A MEG neurophenomenology study. Neurosci. Conscious. 2016 (1), niw019. https://doi.org/10.1093/nc/niw019.

Ermentrout, G.B., Cowan, J.D., 1979. A mathematical theory of visual hallucination patterns. Biol. Cybern. 34 (3), 137–150. https://doi.org/10.1007/BF00336965.

Fort, L.D., Costines, C., Wittmann, M., Demertzi, A., Schmidt, T.T., 2025. Classification schemes of altered states of consciousness. Neurosci. Biobehav. Rev. 175, 106178. https://doi.org/10.1016/j.neubiorev.2025.106178.

Ganesan, S., Yang, W.F.Z., Chowdhury, A., Zalesky, A., Sacchet, M.D., 2024. Within-subject reliability of brain networks during advanced meditation: an intensively sampled 7 tesla MRI case study. Hum. Brain Mapp. 45 (7), e26666. https://doi.org/10.1002/hbm.26666.

Gattuso, J.J., Perkins, D., Ruffell, S., Lawrence, A.J., Hoyer, D., Jacobson, L.H., Timmermann, C., Castle, D., Rossell, S.L., Downey, L.A., Pagni, B.A., Galvão-Coelho, N.L., Nutt, D., Sarris, J., 2023. Default mode network modulation by psychedelics: A systematic review. Int. J. Neuropsychopharmacol. 26 (3), 155–188. https://doi.org/10.1093/ijnp/pyac074.

Gosseries, O., Marie, N., Lafon, Y., Bicego, A., Grégoire, C., Oswald, V., Vanhaudenhuyse, A., 2024. Exploration of trance states: phenomenology, brain correlates, and clinical applications. Curr. Opin. Behav. Sci. 58, 101400. https://doi.org/10.1016/j.cobeha.2024.101400.

Grégoire, C., Sombrun, C., Lenaif, P., Marie, N., Giovine, A., Walter, M., Gosseries, O., Vanhaudenhuyse, A., 2024. Phenomenological characteristics of auto-induced cognitive trance and Mahorikatan® trance. Neurosci. Conscious. 2024 (1). https://doi.org/10.1093/nc/niae024 niae024.

Hasenkamp, W., Wilson-Mendenhall, C.D., Duncan, E., Barsalou, L.W., 2012. Mind wandering and attention during focused meditation: A fine-grained temporal analysis of fluctuating cognitive states. Neuroimage 59 (1), 750–760. https://doi.org/10.1016/j.neuroimage.2011.07.008.

Hove, M.J., Stelzer, J., Nierhaus, T., Thiel, S.D., Gundlach, C., Margulies, D.S., Van Dijk, K.R.A., Turner, R., Keller, P.E., Merker, B., 2016. Brain network reconfiguration and perceptual decoupling during an absorptive State of consciousness. Cereb. Cortex 26 (7), 3116–3124. https://doi.org/10.1093/cercor/bhv137.

Huels, E.R., Kim, H., Lee, U., Bel-Bahar, T., Colmenero, A.V., Nelson, A., Blain-Moraes, S., Mashour, G.A., Harris, R.E., 2021. Neural correlates of the shamanic State of consciousness. Front. Hum. Neurosci. 15, 610466. https://doi.org/10.3389/fnhum.2021.610466.

Kamada, T., Kawai, S., 1989. An algorithm for drawing general undirected graphs. Inf. Process. Lett. 31 (1).

Kay, S.R., Fiszbein, A., Opler, L.A., 1987. The positive and negative syndrome scale (PANSS) for schizophrenia. Schizophr. Bull. 13 (2), 261–276. https://doi.org/10.1093/schbul/13.2.261.

Lanfranco, R.C., Rivera-Rei, Á., Huepe, D., Ibáñez, A., Canales-Johnson, A., 2021. Beyond imagination: hypnotic visual hallucination induces greater lateralised brain activity than visual mental imagery. Neuroimage 239, 118282. https://doi.org/10.1016/j.neuroimage.2021.118282.

Lewis-Healey, E., Tagliazucchi, E., Canales-Johnson, A., Bekinschtein, T.A., 2024. Breathwork-induced psychedelic experiences modulate neural dynamics. Cereb. Cortex 34 (8), bhae347.

Mainieri, A.G., Peres, J.F.P., Moreira-Almeida, A., Mathiak, K., Habel, U., Kohn, N., 2017. Neural correlates of psychotic-like experiences during spiritual-trance state. Psychiatry Res.: Neuroimaging 266, 101–107. https://doi.org/10.1016/j.pscychresns.2017.06.006.

Mateos, D.M., Guevara Erra, R., Wennberg, R., Perez Velazquez, J.L., 2018. Measures of entropy and complexity in altered states of consciousness. Cogn. Neurodynamics 12 (1), 73–84. https://doi.org/10.1007/s11571-017-9459-8.

Mindlin, I., Herzog, R., Belloli, L., Manasova, D., Monge-Asensio, M., Vohryzek, J., Escrichs, A., Alnagger, N., Núñez, P., Gosseries, O., Kringelbach, M.L., Deco, G., Tagliazucchi, E., Naccache, L., Rohaut, B., Sitt, J.D., Sanz Perl, Y., 2024. Whole brain modelling for simulating pharmacological interventions on patients with disorders of consciousness. Commun. Biol. 7 (1), 1–13. https://doi.org/10.1038/s42003-024-06852-9.

Miyashita, Y., 1995. How the brain creates imagery: projection to primary visual cortex. Science 268 (5218), 1719–1720. https://doi.org/10.1126/science.7792596.

Oswald, V., Jerbi, K., Sombrun, C., Jitka, A., Martial, C., Gosseries, O., Vanhaudenhuyse, A., 2025. Understanding individual differences in non-ordinary state of consciousness: relationship between phenomenological experiences and autonomic nervous system. Int. J. Clin. Health Psychol. : IJCHP 25 (1), 100552. https://doi.org/10.1016/j.ijchp.2025.100552.

Pessa, A.A.B., Ribeiro, H.V., 2021. ordpy: A Python package for data analysis with permutation entropy and ordinal network methods. Chaos: Interdiscip. J. Nonlinear Sci. 31 (6), 063110. https://doi.org/10.1063/5.0049901.

Petitmengin, C., 2006. Describing one?S subjective experience in the second person: an interview method for the science of consciousness. Phenomenol. Cogn. Sci. 5 (3–4), 229–269. https://doi.org/10.1007/s11097-006-9022-2.

Quigley, K.S., Kanoski, S., Grill, W.M., Barrett, L.F., Tsakiris, M., 2021. Functions of interoception: from energy regulation to experience of the self. Trends Neurosci. 44 (1), 29–38. https://doi.org/10.1016/j.tins.2020.09.008.

Rogerson, R.G., Barnstaple, R.E., DeSouza, J.F., 2021. Neural correlates of a trance process and alternative states of consciousness in a traditional healer. Brain Sci. 11 (4), 497. https://doi.org/10.3390/brainsci11040497.

Roseman, L., Demetriou, L., Wall, M.B., Nutt, D.J., Carhart-Harris, R.L., 2018. Increased amygdala responses to emotional faces after psilocybin for treatment-resistant depression. Neuropharmacology. 142, 263–269. https://doi.org/10.1016/j.neuropharm.2017.12.041.

Salomon, R., Ronchi, R., Dönz, J., Bello-Ruiz, J., Herbelin, B., Martet, R., Faivre, N., Schaller, K., Blanke, O., 2016. The insula mediates access to awareness of visual stimuli presented synchronously to the heartbeat. J. Neurosci.: Off. J. Soc. Neurosci. 36 (18), 5115–5127. https://doi.org/10.1523/JNEUROSCI.4262-15.2016.

Seitzman, B.A., Gratton, C., Marek, S., Raut, R.V., Dosenbach, N.U.F., Schlaggar, B.L., Petersen, S.E., Greene, D.J., 2020. A set of functionally-defined brain regions with improved representation of the subcortex and cerebellum. Neuroimage 206, 116290. https://doi.org/10.1016/j.neuroimage.2019.116290.

Siegel, R.K., 1977. Hallucinations. Sci. Am. 237 (4), 132–140. https://doi.org/10.1038/scientificamerican1077-132.

Siegel, R.K., Jarvik, M.E., 1975. Drug-induced hallucinations in animals and man. Hallucinations: Behav. Exp. Theory 81, 161.

Smigielski, L., Scheidegger, M., Kometer, M., Vollenweider, F.X., 2019. Psilocybin-assisted mindfulness training modulates self-consciousness and brain default mode network connectivity with lasting effects. Neuroimage 196, 207–215. https://doi.org/10.1016/j.neuroimage.2019.04.009.

Stamatakis, E.A., Adapa, R.M., Absalom, A.R., Menon, D.K., 2010. Changes in resting neural connectivity during propofol sedation. PLoS. One 5 (12), e14224. https://doi.org/10.1371/journal.pone.0014224.

Stawarczyk, D., Majerus, S., Maj, M., Van der Linden, M., D'Argembeau, A., 2011. Mind-wandering: phenomenology and function as assessed with a novel experience sampling method. Acta Psychol. 136 (3), 370–381. https://doi.org/10.1016/j.actpsy.2011.01.002.

Stoliker, D., Novelli, L., Vollenweider, F.X., Egan, G.F., Preller, K.H., Razi, A., 2024. Neural mechanisms of resting-State networks and the amygdala underlying the cognitive and emotional effects of psilocybin. Biol. Psychiatry. https://doi.org/10.1016/j.biopsych.2024.01.002.

Tagliazucchi, E., Roseman, L., Kaelen, M., Orban, C., Muthukumaraswamy, S.D., Murphy, K., Laufs, H., Leech, R., McGonigle, J., Crossley, N., Bullmore, E., Williams, T., Bolstridge, M., Feilding, A., Nutt, D.J., Carhart-Harris, R., 2016. Increased global functional connectivity correlates with LSD-induced ego dissolution. Curr. Biol. 26 (8), 1043–1050. https://doi.org/10.1016/j.cub.2016.02.010.

Tagliazucchi, E., van Someren, E.J.W., 2017. The large-scale functional connectivity correlates of consciousness and arousal during the healthy and pathological human sleep cycle. Neuroimage 160, 55–72. https://doi.org/10.1016/j.neuroimage.2017.06.026.

Tart, C., 1976. .'The basic nature of altered states of consciousness, A system approach. J. Transpers. Psychol. 1. https://www.atpweb.org/jtparchive/trps-08-76-01-045.pdf.

Timmermann, C., Bauer, P.R., Gosseries, O., Vanhaudenhuyse, A., Vollenweider, F., Laureys, S., Singer, T., Antonova, E., Lutz, A., 2023. A neurophenomenological approach to non-ordinary states of consciousness: hypnosis, meditation, and psychedelics. Trends Cogn. Sci. 27 (2), 139–159. https://doi.org/10.1016/j.tics.2022.11.006.

Timmermann, C., Watts, R., Dupuis, D., 2022. Towards psychedelic apprenticeship: developing a gentle touch for the mediation and validation of psychedelic-induced insights and revelations. Transcult. Psychiatry. https://doi.org/10.1177/13634615221082796.

Tsakiris, M., Critchley, H., 2016. Interoception beyond homeostasis: affect, cognition and mental health. Philos. Trans. R. Soc. B: Biol. Sci. 371 (1708), 20160002. https://doi.org/10.1098/rstb.2016.0002.

Vanhaudenhuyse, A., Castillo, M.-C., Martial, C., Annen, J., Bicego, A., Rousseaux, F., Sanz, L.R.D., Sombrun, C., Bioy, A., Gosseries, O., 2024. Phenomenology of auto-induced cognitive trance using text mining: A prospective and exploratory group study. Neurosci. Conscious. 2024 (1), niae036. https://doi.org/10.1093/nc/niae036.

Whitfield-Gabrieli, S., Nieto-Castanon, A., 2012. *Conn*: A functional connectivity toolbox for correlated and anticorrelated brain networks. Brain Connect. 2 (3), 125–141. https://doi.org/10.1089/brain.2012.0073.

Yang, W.F.Z., Chowdhury, A., Bianciardi, M., van Lutterveld, R., Sparby, T., Sacchet, M. D., 2023. Intensive whole-brain 7T MRI case study of volitional control of brain activity in deep absorptive meditation states. Cereb. Cortex (N. Y. NY) 34 (1), bhad408. https://doi.org/10.1093/cercor/bhad408.